Effect of restrained versus free drying on hygro-expansion of hardwood and softwood fibers and paper handsheet

Niels Vonk · Ron Peerlings · Marc Geers · Johan Hoefnagels

Abstract Earlier work on the hygro-expansion of paper states that the larger hygro-expansivity of freely compared to restrained dried handsheets is due to structural differences between the fibers inside the handsheet. To study this hypothesis, first, the hygro-expansion of freely and restrained dried, hardwood and softwood handsheets has been characterized. Subsequently, the transient full-field hygro-expansion (longitudinal, transverse, and shear strain) of fibers extracted from these handsheets was measured using global digital height correlation, from which the micro-fibril angle was deduced. The hygro-expansivity of each individual fiber was tested before and after a wetting period, during which the fiber's moisture content is maximized, to analyze if a restrained dried fiber can "transform" into a freely dried fiber. It was found that the longitudinal hygro-expansion of the freely dried fibers is significantly larger than the restrained dried fibers, consistent with the sheet-scale differences. The difference in micro-fibril angle between the freely and restrained dried fibers is a possible explanation for this difference, but merely for the hardwood fibers, which are able to "transform" to freely dried fibers after being soaked in water. In contrast, this "transformation" does not happen in softwood fibers, even after full immersion in water for a day. Various mechanisms have been studied to explain the observations on freely and restrained dried hardwood and softwood, fiber and handsheets including analysis of the fibers' lumen and cross-sectional shape. The presented results and discussion deepens the understanding of the differences between freely and restrained dried handsheets.

Introduction

Paper is a composite material consisting of natural fibers, e.g., hardwood or softwood. The extreme deterioration of paper's mechanical and geometrical properties due to moisture poses one of the key problems in its exploitation, possibly resulting in non-usable end products. Therefore, being able to control the moisture-induced dimensional stability of paper remains a great challenge. This is especially true for printing applications, during which paper is subjected to multiple drying and wetting cycles while being, respectively, constrained and unconstrained. Failure to control the paper sheet deformation can result in out-of-plane deformations, including curling,

N. Vonk · R. Peerlings · M. Geers · J. Hoefnagels (✉)
Department of Mechanical Engineering, Eindhoven University of Technology, Eindhoven, The Netherlands
e-mail: J.P.M.Hoefnagels@tue.nl

cockling, fluting and waviness (Kulachenko et al. 2005; De Böck et al. 2017), which are driven by processes occurring in the fibrous microstructure, down to the single fiber level. The severity of these out-of-plane deformations are linked to the magnitude of the moisture-induced dimensional change (hygro-expansion) of the paper sheet.

Before addressing the hygro-expansivity of paper, first the paper fiber structure is briefly discussed. Paper fibers are open tube-like structures with a tube wall that consists of four layers (P, S1, S2, S3) made of cellulose, hemi-celluloses and lignin (Liitiä et al. 2000; Hubbe 2014). The lumen, i.e. the tube opening, may be collapsed according to the fiber's processing conditions, i.e. pulping, refining, or paper drying pressure (He et al. 2003; Hubbe et al. 2007; Hubbe 2014). The S2 layer constitutes approximately 80% of the fiber wall (Courchene et al. 2006; Neagu et al. 2006), and is likely to dominate the fiber's hygro-mechanical properties. Each layer is built of long parallel cellulose strands, called micro-fibrils, which alternate between crystalline (40−60 vol%) and so-called "dislocated regions" (Agarwal et al. 2013). These micro-fibrils are helically oriented in each sub-layer, and are stiffer than the hemi-celluloses and lignin counterparts that bind the micro-fibrils into the layer (Salmén 1982; Haslach 2000; Fahlén and Salmén 2005; Berglund 2011; Hubbe 2014). The angle between the micro-fibrils' axis and fiber's longitudinal axis is called the micro-fibril angle (MFA), which is different for each layer and for each wood type. The MFA (of the S2 layer) of hardwood, such as Eucalyptus, is between 0 and 11°, whereas softwood, such as a mixture of Spruce and Pine, typically has a (much) higher MFA ranging from 8 to 39° (French et al. 2000; Barnett and Bonham 2004; Cown et al. 2004; Donaldson 2008). The significantly larger variation in MFA observed for softwood fibers is due to the large difference in MFA between early-, late- and compression wood fibers (Gorisek and Torelli 1999; Anagnost et al. 2002; Jordan et al. 2005). Since the MFA is low for most fibers, the fiber exhibits strong anisotropic hygro-mechanical properties (Retulainen et al. 1998), i.e., a longitudinal to transverse stiffness ratio of 6−11 as found in experiments (Czibula et al. 2021) and used in models (Magnusson and Östlund 2013; Brandberg et al. 2020). Furthermore, the fibers exhibit a longitudinal to transverse hygro-expansion ratio of 20−40 (Wahlström 2009; Joffre et al. 2016;

Vonk et al. 2021). The key challenge now remains how these strongly anisotropic fiber properties translate to the network-scale hygro-expansion, where, e.g., in the bonded areas a competition between the fibers arises.

During paper sheet wetting, the longitudinal fiber hygro-expansion directly contributes to the sheet-scale hygro-expansion through the extension of the freestanding segments. The much larger transverse strain only contributes indirectly to the sheet by transmission through the inter-fiber bonds to the longitudinal extension of the adhered fibers (Brandberg et al. 2020). Theoretical and numerical models have shown that the transverse fiber strain contribution to the sheet scale is relatively weak, i.e. the longitudinal fiber hygro-expansivity dominates (Uesaka 1994; Motamedian and Kulachenko 2019; Brandberg et al. 2020). However, experimental evidence, i.e. large-scale sheet hygro-expansivity and small-scale longitudinal and transverse hygro-expansivity of fibers extracted from these sheets, is lacking, whereas these experiments are essential for tailoring the paper structure to improve its dimensional stability. Lindner (2018) wrote an outstanding review on factors affecting the dimensional stability of paper, in which, the author indicated that increasing the level of restrained drying strongly reduces the hygro-expansivity of paper. However, the driving mechanisms behind these phenomena are under debate, which constitutes the main objective of this work.

The effect of drying restrained on the hygro-mechanical properties of paper has been extensively studied since 1950 (Smith 1950; Brecht et al. 1956a, b). Generally, two paper types are considered when investigating the effect of a drying restraint; machine paper with fibers oriented in the machine direction (MD) making the hygro-mechanical behavior anisotropic, and handsheets which have a random fiber orientation and isotropic behavior. For commercial machine paper making, tension is applied in MD (Nanko and Wu 1995; Mäkelä 2009), inducing a restrained MD, but, depending on the draw, also a restrained CD. Regarding handsheet paper making, restrained dried (RD) handsheets are formed by applying a constant out-of-plane pressure to wet webs, while freely dried (FD) handsheets are typically formed by drying the wet web in between PTFE meshes (Uesaka and Qi 1994; Fellers 2007; Larsson and Wågberg 2008; Urstöger et al. 2020).

After RD paper formation, dried-in strain is stored inside the paper, which upon introduction of moisture is released, resulting in an irreversible shrinkage (Uesaka et al. 1992; Larsson and Wågberg 2008). Interestingly, in (Vonk et al. 2021, 2020), it was found that this release of dried-in strain actually emerges from the single fiber level. Regarding the mechanical properties, lab-made machine paper which was restrained in both CD and MD exhibits a higher specific modulus in both directions compared to FD machine paper (Uesaka and Qi 1994), and the same is found for handsheets, where RD handsheets exhibit a lower strain to failure and larger Young's modulus than FD (Mäkelä 2009; Kouko et al. 2014; Urstöger et al. 2020). Regarding hygro-expansivity, machine paper dried under restrained in CD and MD exhibits a smaller hygro-expansivity than FD machine paper (Uesaka and Qi 1994). Similarly, RD handsheets exhibit a significantly smaller hygro-expansivity than FD handsheets (Salmén et al. 1987, 1987; Uesaka et al. 1992; Nanri and Uesaka 1993; Fellers 2007; Larsson and Wågberg 2008; Urstöger et al. 2020). Hence, RD increases the Young's modulus and dimensional stability of machine paper (in MD and CD) and handsheets compared to FD. The open scientific question that remains is what drives these differences. This work focuses on unraveling the mechanics governing the hygro-expansivity.

Uesaka and Qi (1994) stated that the fibers constituting the inter-fiber bonds inside FD handsheets are more wrapped around each other than their RD handsheet counterparts, due to the absence of an external applied pressure for FD. Consequently, the increased bonded surface would result in a larger transverse strain transfer in the bonded region. This theory is adopted in a few other works (Nanko and Wu 1995; Fellers 2007; Larsson and Wågberg 2008). However, recent work by Urstöger et al. (2020) demonstrated, using 3D X-ray computed tomography characterization of the inter-fiber bond geometries, that the difference in wrap around angle inside FD and RD handsheets is negligible and not significant enough to explain the large hygro-expansivity magnitudes.

In older works, Van den Akker (1961) convincingly argued, based on machine paper experiments, that the difference in mechanical properties between the CD and MD can not solely be explained by the fiber orientation, but are expected to be caused by differences in the drying procedure (i.e. constrained during drying). Jentzen (1964) showed strong evidence that fibers dried under a constant tensile stress reveal a higher Young's modulus than fibers dried under no stress. The author attributed this to the lower MFA of fibers dried under stress. This would mean that changes in the fiber's structure cause the difference in mechanical properties. Interestingly, Meylan (1972) and Yamamoto et al. (2001) showed, for wood fibers, that the magnitude of longitudinal fiber shrinkage decreases for decreasing MFA, which, combined with the work of Nanko and Wu (1995) showing that fibers dried in MD exhibit a lower longitudinal shrinkage than fibers in CD, might suggest that the fibers' structural differences affect the fibers' hygro-expansivity and consequently explains the hygro-expansivity difference of FD and RD paper sheets. Additionally, Salmén et al. (1987) proposed a theory on how dried-in strain is stored inside the amorphous hemi-cellulose and "dislocated cellulose regions" of the fiber and how this affects the hygro-expansivity of the fiber itself. In order to test if structural changes in the fibers can explain the hygro-expansivity differences, one should test single fibers extracted from FD and RD paper and relate the findings at the micro-(fiber) and macro-scale (sheet).

Accordingly, in this work the hygro-expansivity of fibers isolated from either RD or FD handsheets, made of either hardwood or softwood, are tested using a recently developed full-field hygro-expansivity method (Vonk et al. 2020), and compared to the sheet-scale hygro-expansivity. Furthermore, all fibers are loaded to maximum moisture content to determine the release of dried-in strain. Surprisingly, not all fibers are able to release their dried-in strain, and hence additional experiments considering the fiber structure are performed. This approach enables (i) investigation of the mechanisms driving the hygro-expansivity difference, (ii) direct fiber to sheet hygro-expansivity comparison, allowing to distinguish the longitudinal and transverse fiber hygro-expansion contribution to the sheet scale. In this work, first the handsheet and fiber preparation is elaborated, followed by the specific testing procedure of the handsheets and fibers. Then the results are given and discussed in which some additional experiments are elaborated, and, finally, the main conclusions are given[1].

---

[1] Note that a few preliminary experiments of this work have already been reported in (Vonk et al. 2023b), including the hygro-expansion of fibers extracted from hardwood

Materials and methods

Preparation of the handsheets

FD and RD handsheets with an average weight of ∼ 60 g/m² produced from fully bleached hardwood (HW) kraft pulp (Eucalyptus, fiber length: ∼ 900 μm, fiber width: ∼ 15 μm, $\kappa < 2$, unrefined) and fully bleached softwood (SW) kraft pulp (mixture of Spruce and Pine, fiber length: ∼ 2000 μm, fiber width: ∼ 30 μm, $\kappa < 2$, unrefined), using the "Rapid Kötchen" device, were kindly provided by *Mondi Group, Austria*. The method proposed by Larsson and Wågberg (2008) was followed; the FD handsheets were once pressed for 1 min with a temperature (*T*) of 93 °C and pressure of 95 kPa and afterwards freely dried in a PTFE mesh drying frame consisting of stabilizing bars. The RD handsheets were pressed for 10 min with a *T* of 93 °C and pressure of 95 kPa. Note that the used HW and SW pulps (stored at RH = 50% and *T* = 23 °C) are the same as used for the single fiber hygro-expansion experiments conducted in (Vonk et al. 2021), thus enabling direct comparison of results. Each handsheet was subsequently cut into 6×6 cm² sheets and a random speckle pattern was applied using charcoal sticks as shown in Fig. 2, instead of using spray paint, of which the solvent could affect the paper structure. The speckle pattern is required for a Global Digital Image Correlation (GDIC) algorithm as proposed by Neggers et al. (2016) to track the displacement field, which enables identification of the in-plane hygro-expansion.

Preparation of the single fibers

From the handsheets a total of, respectively, five FD and twelve RD HW fibers and ten FD and ten RD SW fibers were extracted by means of delaminating the paper sheet and cutting the naturally sticking out fibers (Hirn and Bauer 2006). For these sample fibers, only fibers without any noticeable pre-deformation or damage were accepted. Moreover a comprehensive analysis on 100 fibers picked from the handsheets

showed that the morphology of the fibers was completely random in terms of straightness, twist, etc. confirming that the fiber extraction procedure did not select specific fibers, and consequently, the fibers tested are also of random nature. For the tests, each fiber is delicately clamped using two nylon threads following the method proposed in (Vonk et al. 2020), as schematically shown in Fig. 1b₁. To enable Global Digital Height Correlation (GDHC) (Vonk et al. 2020), a micro-particle pattern was applied by exposing the fiber to a mist of freely floating sub-micro particles, created with a mystification setup (Shafqat and Hoefnagels 2021).

Single fiber hygro-expansivity experiments

The fibers (one by one) were subsequently tested inside a climate chamber underneath an optical profilometer, in which the RH is varied following a specific trajectory (Fig. 1a) using a RH sensor (feedback control) located approximately 4 cm from the fiber (closer is not possible to avoid collision), during which the 3D deformation of the fiber is captured (one topography per 30 s). The fiber is clamped on a flow-through element (Fig. 1b₂) which is connected to an external water temperature regulator enabling temperature control of the specimen. Examples of *in situ* acquired topographies in the dry and wet state are shown in Fig. 1c. After testing, GDHC, a topography correlation algorithm (Vonk et al. 2020), is used to obtain the full-field fiber deformation, i.e. the longitudinal (ϵ_{ll}), transverse (ϵ_{tt}) and shear hygro-expansion (ϵ_{lt}) field shown in Fig. 1d for the deformation accumulated during the second wetting slope (between 30 and 90% RH) of a SW fiber. The strain fields are subsequently averaged towards a single scalar value of ϵ_{ll}, ϵ_{tt}, and ϵ_{lt}, for each topography in time, enabling visualization of the evolution of the hygro-expansion.

Figure 1a shows two slightly different RH/*T* trajectories that are used to test HW and SW fibers. In both RH/*T* trajectories the fiber is first subjected to (i) two linearly increasing RH cycles from 30−90−30% (cycle 1−2) and temperature of 23 °C, then (ii) a wetting cycle during which the fiber's moisture content is maximized by means of lowering the specimen temperature to 15 °C, (locally) increasing the RH (Fellers 2007), and generating condensation droplets as visible in Fig. 1c₂, and finally (iii) two 30−90−30% RH cycles (cycle 3−4) at a temperature of 23 °C. Each

Fig. 1 Single fiber hygro-expansion experiment (extended ▶ from (Vonk et al. 2020)). **a** The fiber is exposed to a combined relative humidity (RH, black line) and temperature trajectory (T, colored line), which is slightly different for a_1 HW and a_2 SW fibers. b_1 Two nylon threads clamp the fiber for maximum freedom while the region-of-interest remains in the field-of-view of the optical profilometer (b_2), which monitors the fiber topography, starting from the (c_1) dry state to c_2 the fully wet state. **d** The obtained topographies are correlated using GDHC to yield the evolution of the d_1 longitudinal (ϵ_{ll}), d_2 transverse (ϵ_{tt}), and d_3 shear strain field (ϵ_{lt}), shown here for the strain between 30 and 90% RH of the second RH cycle

change in RH set-point is conducted with a slope 1%/min, equal to that of the handsheets. This strategy is chosen to test if an initially RD fiber is able to "transform" into a FD fiber when subjected to sufficient moisture.

The differences between, and details of, the RH/T trajectories of HW and SW displayed in Fig. 1a are explained in Subsection "Fiber RH/T trajectories" (Supplementary information).

Sheet-scale hygro-expansivity experiments

The full-field in-plane paper hygro-expansion method based on GDIC involves placing the patterned paper sheet in between two flat (~ 5 μm corner-to-corner height deviation) woven steel gazes, which are spaced with the paper thickness to minimize out-of-plane deformation, which is known to occur during sheet-scale hygro-expansion measurements (Kulachenko et al. 2005; De Böck et al. 2017), shown in Fig. 2. This paper sheet is tested inside a climate chamber, in which the relative humidity (RH) is regulated, and captured using a telecentric lens-camera setup, as shown in Fig. 2. This setup enables minimization of artificial strains due to out-of-plane deformations, because of the lens' invariant magnification around the focus point. The RH is regulated by an external humidifier (*Cellkraft P-10 series*). In the experiments, two RD and two FD handsheets were tested for HW and SW, with each test consisting of six linearly increasing RH cycles from 30−90−30%, with a slope of 1%/min, resulting in a total duration of 12 h. All (eight) sheets were acclimatized at 30% RH for at least 12 h before testing. Images were captured once per two minutes and were correlated using a GDIC framework with linear shape functions to find the linearly varying evolution of the displacement field corresponding to constant strain fields $\epsilon_{xx}(x, y) = \epsilon_{xx}$,
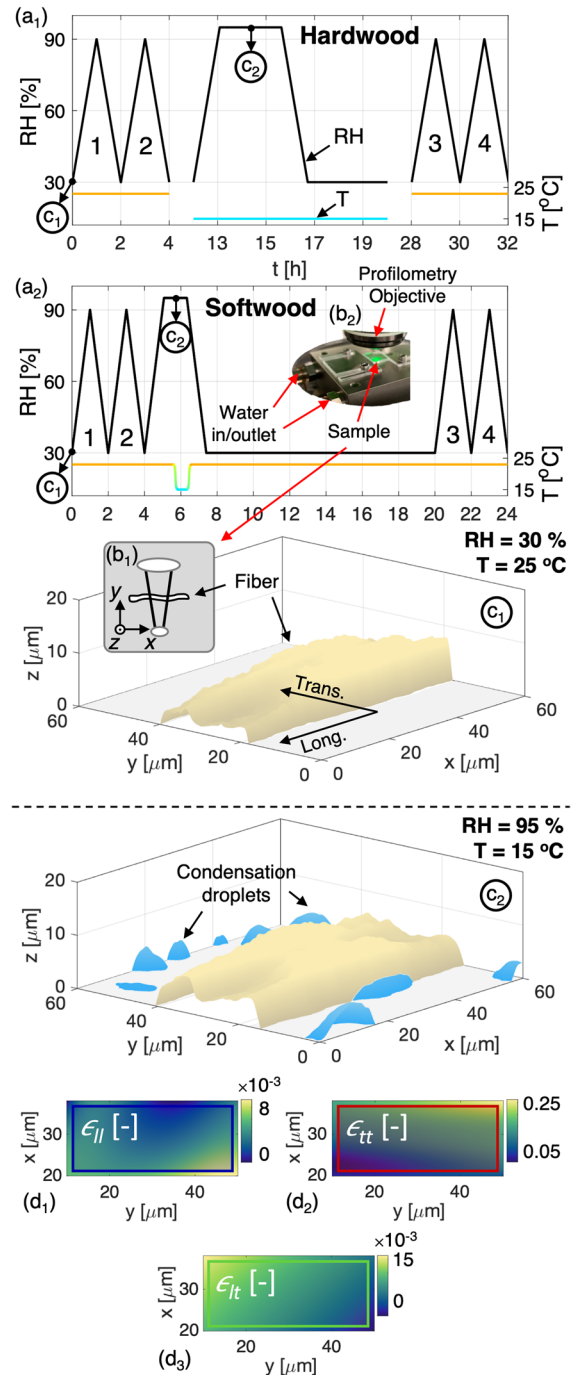
$\epsilon_{yy}(x, y) = \epsilon_{yy}$, and $\epsilon_{xy}(x, y) = \epsilon_{xy}$ (Neggers et al. 2016). As ϵ_{xy} remains zero and ϵ_{xx} equals ϵ_{yy} within uncertainty margins, the sheet hygro-expansion is computed as $\epsilon_s = (\epsilon_{xx} + \epsilon_{yy})/2$. Note that GDIC is a 2D formulation, while GDHC, which is used for the fiber hygro-expansivity below, is a quasi-3D
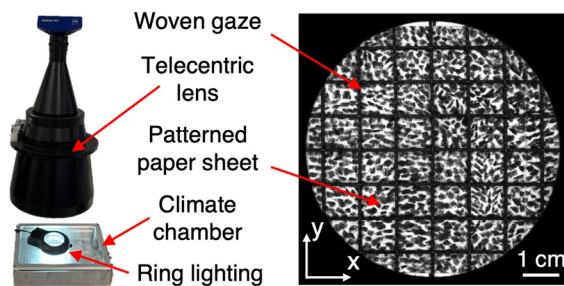
Fig. 2 Paper sheet-scale hygro-expansion setup, consisting of a climate chamber underneath a telecentric lens-camera setup. This specific lens annihilates artificial strain due possible present out-of-plane deformations. The patterned paper sheet is placed in between two flat (~ 5 μm corner-to-corner height deviation) woven gazes to minimize out-of-plane deformation to further minimize artificial strains

framework. Finally, local DIC, which is more common (also commercially available), has been used earlier for multiple paper mechanics problems, e.g., paper sheet-scale hygro-expansion measurements (Fellers 2007) and strain field evolution of paper sheets subjected to bi-axial tension (Alzweighi et al. 2022). Here GDIC is adopted as it is more accurate for low spatial variations in the strain field.

Results and discussion

The produced RD handsheets exhibited a significantly lower hygro-expansion than the FD handsheets, as will be shown below in Fig. 11, similar to other work in the literature, indicating that the handsheet fabrication process was conducted as expected. The fiber hygro-expansion is elaborated first because this reveals the most novel and interesting results in terms of hygro-expansivity, which will be later on compared to the sheet-scale hygro-expansion.

Evolution of the fiber hygro-expansivity

The hygro-expansion response of a typical FD and RD, HW and SW fiber is given in Fig. 3. The strong anisotropic swelling behavior of the fibers is directly visible. Optimization of the fiber preparation and testing method have resulted in a significantly better strain resolution compared to Vonk et al. (2020), whereby the precision improved from $1 \cdot 10^{-4}$ and $7 \cdot 10^{-4}$ in longitudinal and transverse direction

respectively, to $1 \cdot 10^{-4}$ and $2 \cdot 10^{-4}$ (Vonk et al. 2023b). Furthermore, some fibers (e.g., FD SW fiber) show scattered data during the wetting cycle, which is caused by severe condensation occurring at the fiber surface (and possibly the particles), making the GDHC unstable. Nevertheless, the global curve is still visible and reliable, because all final solutions of the GDHC converged properly. This indicating that the obtained deformation fields correctly connect the deformed and undeformed configurations, otherwise proper convergence cannot be warranted. Note that the fiber method enables monitoring the surface strain field during the transition to an almost fully wet surface, during the wetting cycle itself, and during the reversed transition to a dry surface (which will be studied in more detail in (Vonk et al. 2023a).

Interestingly, at the end of the wetting cycle, when the RH is decreasing, the hygro-expansion is lagging behind the RH decrease (most prominently visible for the HW fibers) due to the severe condensation present around the fiber, requiring time to evaporate. The condensation around the fiber results in an unknown RH value near the fiber, which is not a concern because the purpose of this wetting cycle is to characterize the release of dried-in strain before and after this period, for which a long period of high moisture content levels is required. The moment at which the condensation initiates shows a rather high variability for the original RH/T procedure applied to the HW fibers. For the adapted RH/T procedure applied to the SW fibers, no droplet formation is visible during the 30 min at 95% RH and high temperature, but lowering the stage temperature immediately initiates droplet formation and consequently increases the fibers' moisture content, characterized by the rise in ϵ_{tt} (also slight increase in ϵ_{ll}) of both SW fibers in Fig. 3. This is the moment where the fiber exhibits hydro-expansion instead of the initially studied hygro-expansion (Larsson et al. 2009). The strength of the approach lies in the fact that the hygro- and hydro-expansion of the same type of fiber within the same experiment can be studied. For almost all fibers, the hydro-expansivity entails significantly larger strains compared to the hygro-expansion induced during RH cycles 1−2, except for a few fibers exhibiting severe shrinkage during the wetting period, confirming that a higher moisture content is reached. All fibers tend to reach an equilibrium during the wetting cycle (although some small, random variations in the order of ~10^{-3}
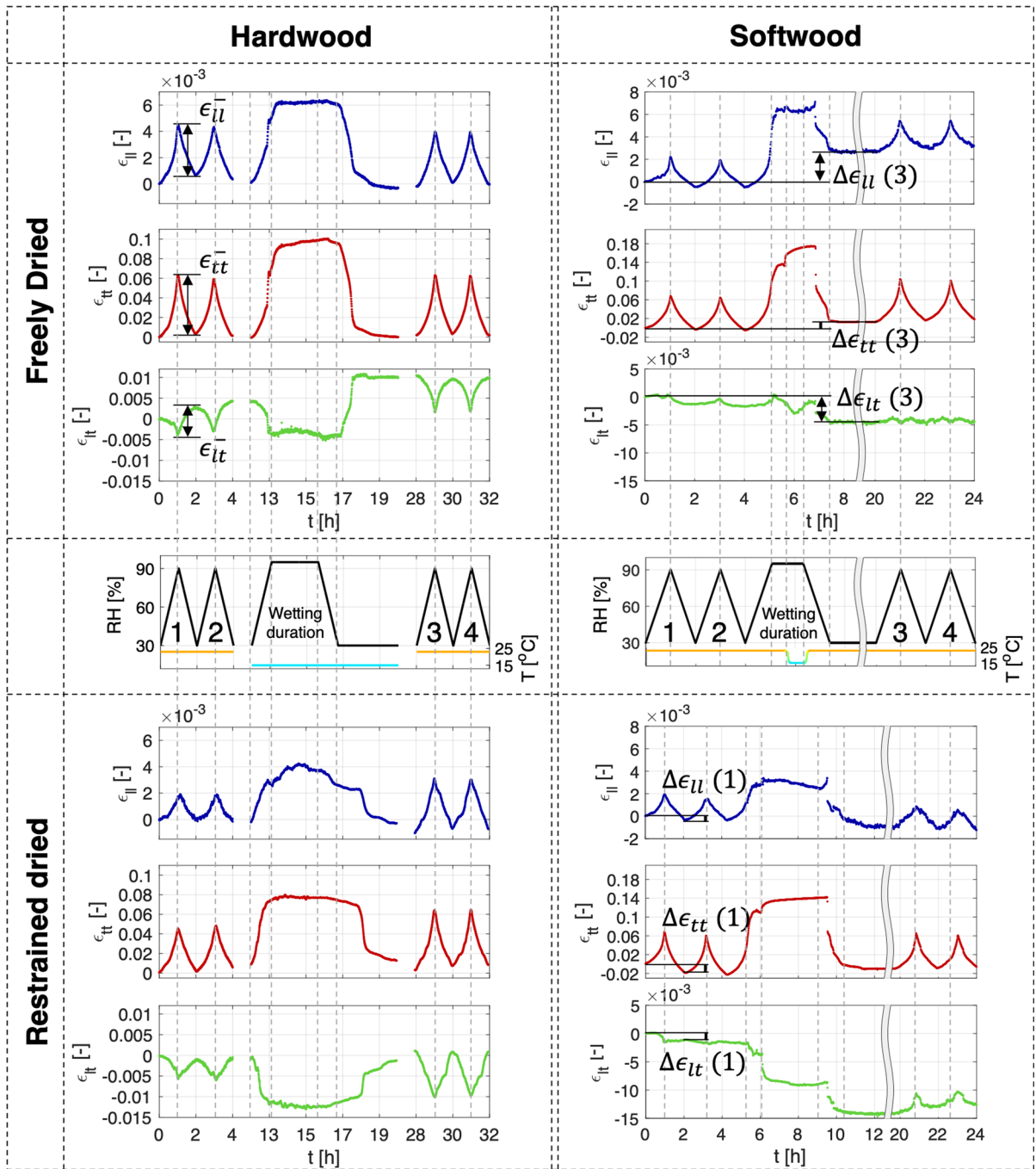
Fig. 3 The longitudinal (ϵ_{ll}), transverse (ϵ_{tt}) and shear hygro-expansion (ϵ_{lt}) evolution of a typical SW and HW, RD and FD fiber. The delay between the hygro-expansion and the RH is due to the presence of condensation. The cooling time during the wetting cycle of the RD SW fiber was slightly longer than the FD SW fiber because the condensation formation took longer. The release of dried-in strain ($\Delta\epsilon$) between the start and (i) after the first RH cycle (1, in the RD SW curve), and (ii) just before the third RH cycle, after the wetting cycle (3, in the FD SW curve) are extracted and shown in Fig. 4. The change in strain for each drying slope from 90 to 30% RH (ϵ_{ll}^-, ϵ_{tt}^-, and ϵ_{lt}^- depicted in the FD HW curve) is extracted for each RH cycle for further analysis
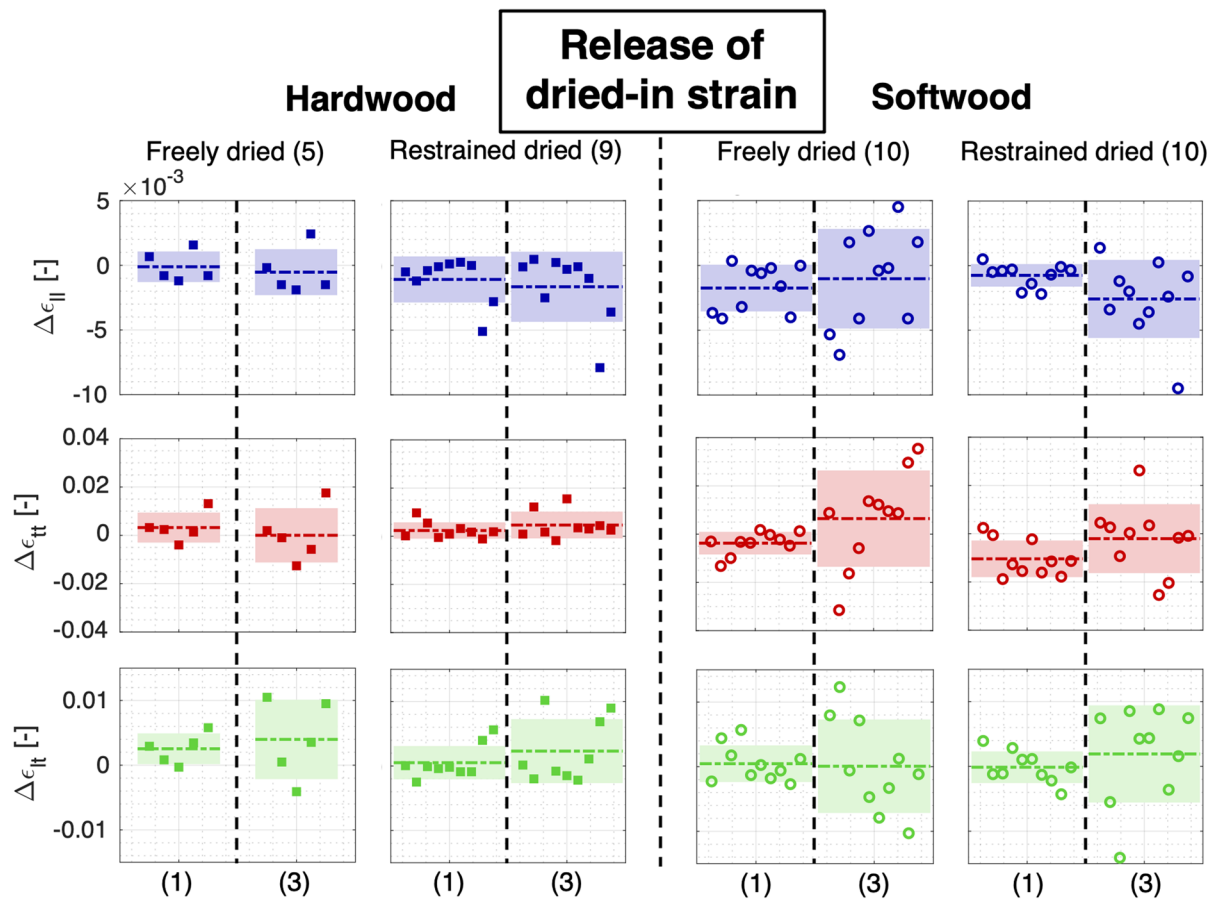
Fig. 4 The release of dried-in strain in longitudinal (ϵ_{ll}), transverse (ϵ_{tt}), and shear direction (ϵ_{lt}) after the first RH cycle, labeled (1) in Fig. 3, and just before the third cycle, after the wetting cycle, labeled (3) in Fig. 3. The values are separately given per fiber, together with the average and standard deviation of all fibers, represented by the dashed line and colored band respectively

strain remain, showing that the strain accuracy is approximately one order of magnitude lower for a full wet surface compared to a dry surface at lower RH levels), implying saturation of the moisture content and full release of dried-in strain. The transient fiber hydro-expansion during the wetting cycle is studied in more detail in (Vonk et al. 2023c).

Release of dried-in strain

All fibers show a clear release of dried-in strain during the wetting slope of RH cycle 1, because it deviates from the subsequent wetting slopes, similar to earlier single fiber hygro-expansion measurements (Vonk et al. 2021, 2020, 2023b) and earlier sheet-scale hygro-expansion works (Uesaka et al. 1992;

Larsson and Wågberg 2008; Urstöger et al. 2020; Vonk et al. 2023b), as well as the sheet-scale experiments shown later in Fig. 11. More interestingly, all fibers show a release of dried-in strain after the wetting cycle, visible in the fact that for each fiber at least one of the three strain components shows a large difference between the start of the wetting cycle and the start of RH cycle 3 (at which the temperature and RH are the same as the start of the experiment). The average release of dried-in strain in ϵ_{ll}, ϵ_{tt}, and ϵ_{lt}, i.e., $\Delta\epsilon_{ll}$, $\Delta\epsilon_{tt}$, and $\Delta\epsilon_{lt}$ after RH cycle 1, labeled (1), and between the start and just before RH cycle 3, labeled (3), considering all fibers, are presented in Fig. 4.

The values per fiber are given separately, and the average and standard deviation of all fibers visualize the global trend. Clearly, not all dried-in strains

are released after the first RH cycle (1), because the dried-in strain after the wetting cycle (3) is on average larger. Hence, dried-in strains are still stored inside the fiber after being subjected to 90% RH. Furthermore, all groups of fibers show both positive and negative $\Delta\epsilon_{ll}$ values, implying that the fibers inside both FD and RD handsheets experienced drying under compression or tension. However, more fibers inside the FD handsheets were dried under compression characterized by the larger number of positive dried-in strain values. These results are in line with Nanko and Wu (1995), who showed that non-bonded fiber segments at the paper surface experienced either swelling or shrinkage during FD and RD depending on their neighboring fibers, and the FD case showed more drying under compression. Furthermore, the larger $\Delta\epsilon_{ll}$ for RD compared to FD is attributed to the sheet dryer exerting an out-of-plane compression on the sheet. Thereby imposing a drying (tensile) stress on most fibers, resulting in a larger portion of fibers being dried under tensile stresses. In contrast, during FD, so-called "micro-compressions" may induce in the bonded areas (Page and Tydeman 1962). The scatter in $\Delta\epsilon_{ll}$ is also visible in $\Delta\epsilon_{tt}$ (mainly for SW), suggesting that the applied tensile or compressive stress during drying, respectively, contracts or expands the cross-section of the fibers.

To investigate how the release of dried-in strains and the drying procedure affects the hygro-expansivity of the fibers, the shrinkage before the wetting cycle (i.e. RH cycles 1−2) and after the wetting cycle (i.e. RH cycles 3−4) are extracted and discussed in the following.

Comparison of hygro-expansion magnitudes

The average (with standard deviation) longitudinal and transverse shrinkage, and shear strain change of all FD and RD HW and SW fibers during the drying slope from 90 to 30% RH for cycles 1−2 (before the wetting cycle), i.e. $\bar{\epsilon}_{ll}^-$, $\bar{\epsilon}_{tt}^-$, and $\bar{\epsilon}_{lt}^-$ are shown in Fig. 5. For better analysis, the shrinkage is defined as a positive strain value, i.e. the strain changes are obtained by subtracting the value at 90% by the value at 30%, as annotated for RH cycle 1 of FD HW in Fig. 3. Which results, for this specific hygro-expansion curve, in positive values (shrinkage) for ϵ_{ll}^- and ϵ_{tt}^-, and negative ϵ_{lt}^-. Subsection "Fiber hygro-expansion magnitudes" (Supplementary information) provides

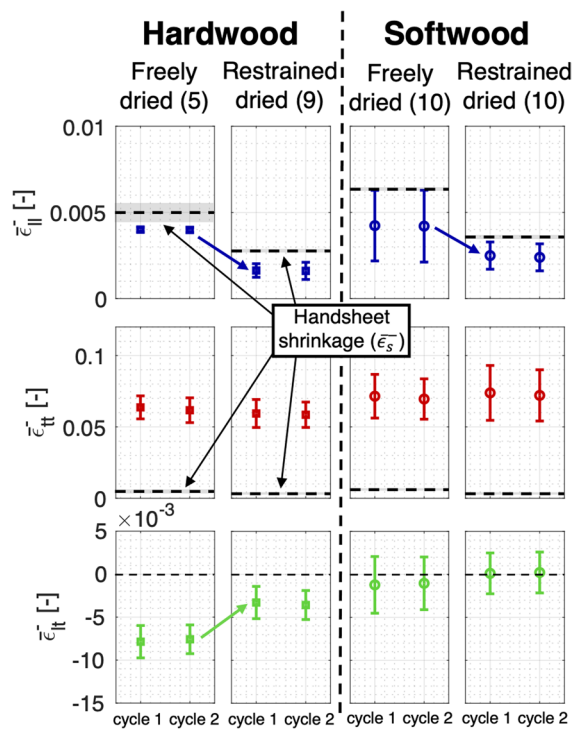**Fig. 5** The average longitudinal (ϵ_{ll}^-) and transverse shrinkage (ϵ_{tt}^-), and shear strain change (ϵ_{lt}^-) during the drying slopes from 90 to 30% RH for cycles 1−2, as annotated for RH cycle 1 of the FD HW fiber in Fig. 3, of all HW (five and nine fibers from the FD and RD HW handsheets respectively) and SW fibers (ten fibers each from the FD and RD SW handsheets), i.e. $\bar{\epsilon}_{ll}^-$, $\bar{\epsilon}_{tt}^-$, and $\bar{\epsilon}_{lt}^-$, including standard deviation. The total average handsheet shrinkage ($\bar{\epsilon}_s^-$, given in Table A.2) is added to the $\bar{\epsilon}_{ll}^-$ plot

(i) the strains per fiber for each cycle separately given in Figures A.1a and A.2a, of which marker numbering is consistent with the dried-in strain releases given in Fig. 4, (ii) the total average shrinkage considering cycles 1−2 of all fibers, and (iii) an explanation why three RD HW fibers are excluded from the analysis and extra details on RD HW fibers which exhibited severe shrinkage during wetting.

All fibers show a low cycle-to-cycle variability when comparing RH cycle 1 to 2, whereas only the HW fibers demonstrate a low fiber-to-fiber variability, similar to results in (Vonk et al. 2021). The latter is attributed to the significantly larger MFA range of the SW compared to the HW fibers (French et al. 2000; Barnett and Bonham 2004; Cown et al. 2004; Donaldson 2008), which is known to correlate to the fiber's hygro-expansivity (Meylan 1972;

Yamamoto et al. 2001). Interestingly, for the SW fibers, the scatter of $\bar{\epsilon}_{ll}^-$ is lower for the RD SW fibers, opposite to what can be expected, which is discussed later.

Regarding the shrinkage, both for HW and SW, the FD fibers show a larger shrinkage than the RD fibers, especially in longitudinal direction. For HW and SW, the RD procedure mainly affects the longitudinal shrinkage and, to a lesser extent, also the shear, while not affecting the transverse shrinkage. On average, the FD HW fibers shrink 2.5 times more in longitudinal and 1.1 times more in transverse direction compared to RD HW fibers, and the shear is 2.3 times larger. The FD SW fibers shrink 1.8 times more in longitudinal and similarly (1.0) in transverse direction than the RD SW fibers, and the shear is 5.5 times less. The large difference of $\bar{\epsilon}_{lt}^-$ of the SW fibers stems from the RD shear strains being close to zero. A t-test revealed that the HW fibers' longitudinal shrinkage and shear between FD and RD are statistically different, while for the SW fibers, only the longitudinal shrinkage between FD and RD is statistically different, considering 98% confidence. Furthermore, the SW fibers exhibit a slightly larger average longitudinal and transverse shrinkage than the HW fibers (t-test: only $\bar{\epsilon}_{tt}^-$ of the RD HW and SW fibers are statistically within 98% confidence), which is in line with the slightly larger sheet-scale shrinkage of SW compared to HW described in Subsection "Fiber-to-sheet coupling" (Supplementary information), and the literature (Nanko and Wu 1995; Uesaka and Moss 1997).

Collectively, because the hygro-expansivities (shrinkage) of the RD and FD fibers are significantly different, it can be expected that the fiber structure itself is different between the RD and FD fibers, which directly affects the sheet hygro-expansion. This is visualized by comparing $\bar{\epsilon}_{ll}^-$ to the average hand-sheet shrinkage, as is done in the $\bar{\epsilon}_{ll}^-$ plot in Fig. 5. Hence, to explain the sheet hygro-expansion differences, it is not needed to introduce geometrical differences that have been hypothesized to occur in the bonded regions (Uesaka 1994), as earlier questioned by Urstöger et al. (2020), supporting the earlier works stating that structural fiber differences are sufficient to explain the sheet-scale differences (Van den Akker 1961; Jentzen 1964; Nanko and Wu 1995). The structural differences and the driving mechanisms of these

hygro-expansivity differences are studied next, where first only HW is considered.

Hardwood fibers: driving mechanism of the hygro-expansivity difference

Jentzen (1964) showed that the MFA of RD fibers is lower than FD fibers. Therefore, it would be insightful if the MFA of each of the above-tested FD and RD, HW and SW fibers can be measured or assessed. Unfortunately, most MFA measurement techniques in literature (i) have insufficient accuracy to detect the small differences in MFA between the FD and RD fibers which are expected to be low, as will be shown later on, while the MFA is known to vary along the fiber length (Ye et al. 1994; Anagnost et al. 2002), and/or (ii) require wood slices (Cave 1997; Wang et al. 2001; Sarén and Serimaa 2006; Donaldson 2008; Zhang et al. 2019). Only one method (proposed by Heinemann and Retulainen (2014)) based on transmission white-light polarization microscopy has been proposed to measure the MFA of individual fibers, which is explored. The method was adopted and further optimized, and now allows determination of the MFA of the full fiber surface instead of a few discrete locations, of which a detailed description and an example figure is given in Subsection "Determination of the micro-fibril angle" (Supplementary information). Unfortunately it was concluded that the method is fundamentally not applicable to paper fibers, because the polarized light travels though the front and back fiber wall of which the micro-fibrils are crossed due to their helical structure, inevitably resulting in an MFA around 0°, as explained in more detail in Subsection "Determination of the micro-fibril angle" (Supplementary information). Finally, Liu et al. (2016) characterized the local MFA of single plant cells using scanning X-ray micro-diffraction, which enables MFA characterization of the FD and RD fibers studied here. However, the access to scanning X-ray micro-diffraction systems is very limited. Nevertheless, as will be shown next the MFA can indirectly be deduced from the full-field fiber hygro-expansion measurements.

In (Vonk et al. 2021) it was demonstrated that computation of the principal strains, by means of an eigenvalue decomposition from the full-field strain tensor with components ϵ_{ll}^-, ϵ_{tt}^-, and ϵ_{lt}^-, enables the determination of not only the major and
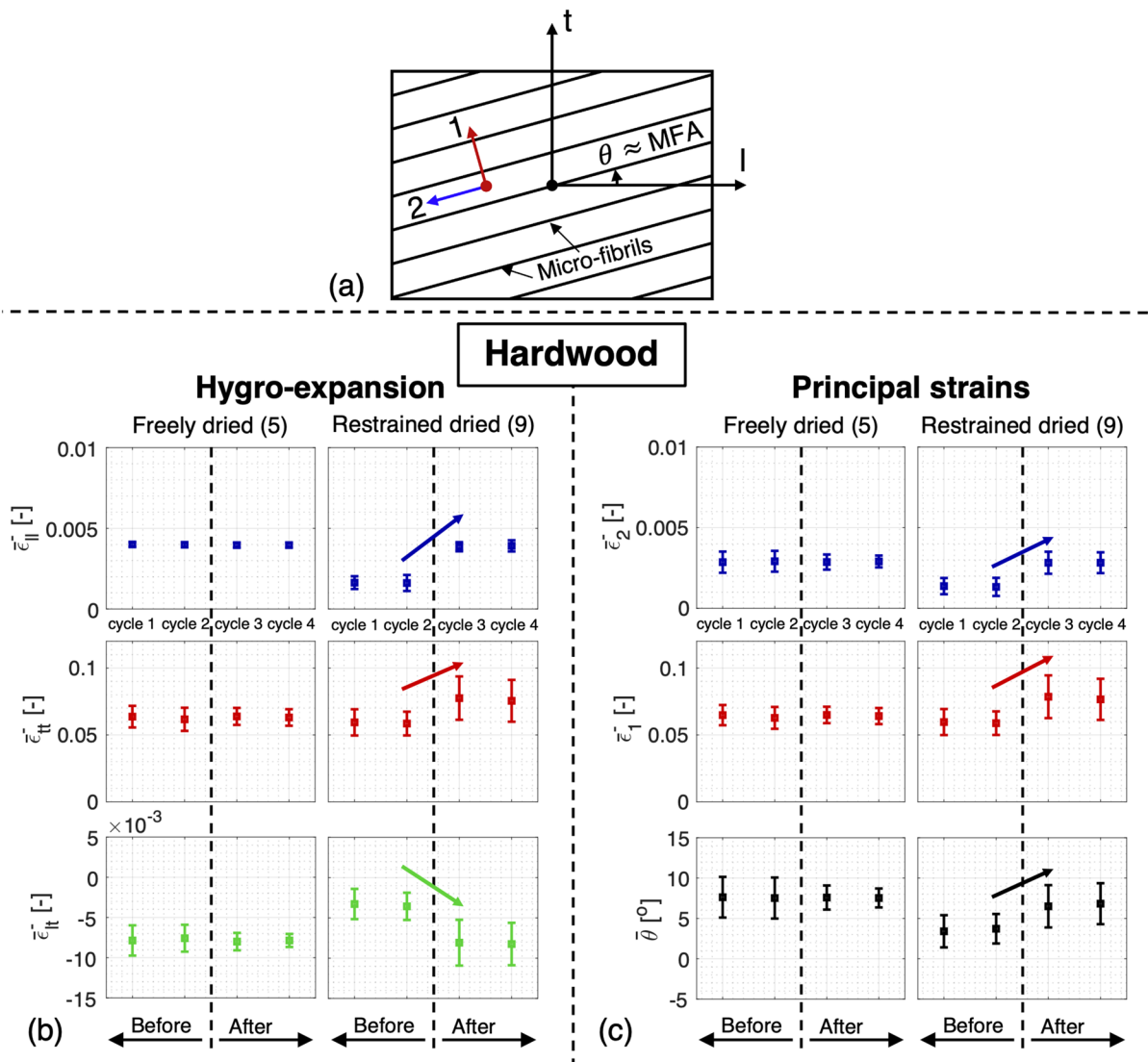
Fig. 6 a Schematic visualization of the principal strains directions with 1 oriented in the direction of the major strain, i.e., perpendicular to the fibril orientation and 2 for the minor strain oriented along the micro-fibrils, and the major-minor strain angle (θ) related to the MFA. **b** The average longitudinal and transverse shrinkage, and shear strain change during the drying slopes from 90 to 30% RH per RH cycle of all HW fibers (five and nine fibers extracted from the FD and RD HW handsheets respectively), i.e. $\bar{\epsilon}_{ll}^-$, $\bar{\epsilon}_{tt}^-$, and $\bar{\epsilon}_{lt}^-$, including standard deviation. **c** The average principal strains and major minor strain angle, i.e. $\bar{\epsilon}_1^-$ and $\bar{\epsilon}_2^-$, and $\bar{\theta}$ are computed from the full-field hygro-expansion, of which θ approximates the MFA

minor strain (ϵ_1, and ϵ_2), but also the in-plane principal strain direction, i.e. the major-minor strain angle (θ). Considering (i) that the fiber's mechanical behavior is dominated by the S2 layer, and (ii) that the direction of major strain will be perpendicular to the relatively stiff micro-fibrils, due to the deformation induced by the swelling of the hemi-celluloses in between the micro-fibrils, the MFA has to be (close

to) perpendicular to the major-minor strain angle, as shown in Fig. 6a. Hence, the average major and minor strain, and the average major-minor strain angle during shrinkage from 90 to 30% RH, i.e. respectively $\bar{\epsilon}_1^-$ and $\bar{\epsilon}_2^-$, and $\bar{\theta}$ are given for all RH cycles along with the regular average strains ($\bar{\epsilon}_{ll}^-$, $\bar{\epsilon}_{tt}^-$, and $\bar{\epsilon}_{lt}^-$) in Fig. 6. The shrinkage and principal strains of all fibers separately are again given in Figure A.1.

Let us first examine RH cycles 1−2, before the wetting cycle. Clearly, all FD and RD HW fibers are within the MFA range reported in the literature, i.e. 0−11 ° (French et al. 2000; Donaldson 2008). Furthermore, the HW fibers show distinctly different values for θ, i.e., 7.57 ± 2.67 and $3.56 \pm 2.92°$ between FD to RD respectively (t-test: statistically different within 98% confidence). This shows that the MFA of the RD HW fibers is indeed lower than the FD fibers, which is in agreement with the findings of Jentzen (1964).

The differences may be rationalized by analyzing the principal strains in Fig. 6c. $\bar{\epsilon}_2^-$ of the FD and RD HW fibers shows that the shrinkage along the fibril length is actually non-zero, indicating that the micro-fibrils themselves can swell or shrink in their longitudinal direction, suggesting that the "dislocated regions" in the cellulose micro-fibrils are indeed accessible to water (Agarwal et al. 2016). $\bar{\epsilon}_2^-$ of the RD HW fibers (RH cycles 1−2) is significantly lower than the FD HW fibers, indicating that the "dislocated cellulose regions" shrink less, mainly affecting the fiber's longitudinal shrinkage due to HW's low MFA (French et al. 2000; Donaldson 2008). These results are in good agreement with the theory of Salmén et al. (1987) who stated, for RD paper, that the "dislocated regions" in the cellulose micro-fibrils are stretched when dried under tension (inducing a residual tensile stress in the direction of the micro-fibrils). This in turn minimizes the swelling of these regions upon wetting, and therefore they contribute less to the fibers' overall hygro-expansivity. For FD fibers, the "dislocated regions" are dried without tension, and thus shrink upon drying, through which they can contribute more to the fiber's hygro-expansivity. Additionally, Kulachenko et al. (2012) showed that the drying procedure also affected the hygro-expansivity of nano-cellulose paper that consists of squared cross-sectional nano-fibrils with a height and width of 20 nm, corresponding to the size of nano-fibril aggregates that form the cell wall of paper fibers (Fahlén and Salmén 2005). The reported difference by Kulachenko et al. (2012) between the FD and RD nano-paper's drying slopes from 80 to 20% RH was ~ 0.20% strain (RD: 0.75% FD: 0.95%), which is similar to the difference in $\bar{\epsilon}_2$ found in Fig. 6c between FD and RD (for an RH change of 90 to 30%). This suggests that this hygro-expansion difference of the nano-cellulosic paper is driven by the swelling

capabilities of the "dislocated regions" in the cellulose nano-fibrils as proposed by Salmén et al. (1987).

The fact that the RD and FD HW fibers show distinctly different values of $\bar{\theta}$, indicates that the MFA of FD fibers is higher than RD fibers, hence constitutes a driving mechanism behind the difference in hygro-expansivity of the HW fibers, similar to the findings of Jentzen (1964). Furthermore, the significant difference in $\bar{\epsilon}_2$ between the RD and FD HW fibers is consistent with the theory by Salmén et al. (1987).

To investigate if the release of dried-in strain is reversible, the shrinkage after the wetting cycle, i.e. RH cycles 3−4 given in Fig. 6 is studied. When comparing RH cycles 1−2 to cycles 3−4, all FD fibers tend to show a similar average values before and after the wetting cycle, although a slight decrease of the scatter of $\bar{\epsilon}_{lt}^-$ and θ is observed. The shrinkage of the RD HW fibers is similar to the FD HW fibers after the wetting cycle (only $\bar{\epsilon}_{tt}^-$ may be slightly larger for the RD HW fibers), indicating that RD HW fibers, when subjected to sufficient water, can "transform" into fibers that exhibit a hygro-expansivity similar to FD HW fibers, which is essential knowledge for paper recyclability. This is, however, in contrast to the experiments conducted in (Vonk et al. 2023b), during which the RD HW fibers were subjected for a long duration to an RH level of 95% but without cooling, resulting in the fiber surface not becoming fully wet. Consequently, the fibers did not completely "transform" to FD fibers, showing the importance of cooling down the specimen to enforce higher moisture content levels of the fibers in order to activate the release of the fiber's dried-in strain. Furthermore, the RD HW fibers in Fig. 6c yield a θ of $6.66 \pm 2.34°$ for RH cycles 3−4, which is equal to RH cycles 1−2 of the FD HW fibers (t-test: statistically not different within 98% confidence), indicating that the change in θ between the two drying procedures is close to reversible. Additionally, $\bar{\epsilon}_2^-$ of the RD HW fibers (RH cycles 3−4) in Fig. 6c is similar to $\bar{\epsilon}_2^-$ of the FD HW fibers, indicating that the shrinkage along the fibril direction increased, giving further support to the theory of Salmén et al. (1987) which states that the difference in swelling capabilities of the "dislocated regions" in the cellulose micro-fibrils between FD and RD affects the fiber's hygro-expansivity. In short, the RD HW fibers can "transform" to fibers exhibiting the characteristics of FD HW fibers.
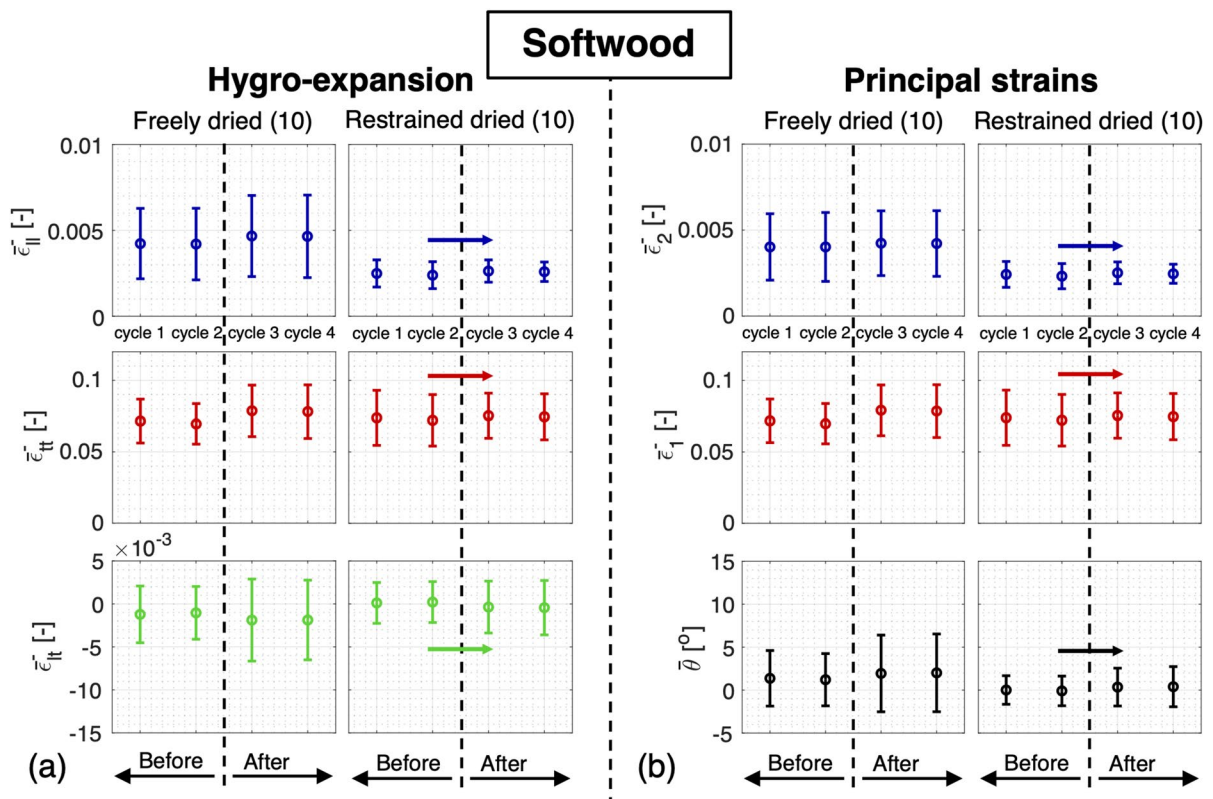
Fig. 7 The average longitudinal and transverse shrinkage, and shear strain change during the drying slopes from 90 to 30% RH per RH cycle of the SW fibers (ten fibers extracted from each FD and RD SW handsheet), i.e. $\bar{\epsilon}_{ll}^-$, $\bar{\epsilon}_{tt}^-$, and $\bar{\epsilon}_{lt}^-$, including standard deviation. The average principal strains ($\bar{\epsilon}_1^-$ and $\bar{\epsilon}_2^-$) and major-minor strain angle ($\bar{\theta}$) are computed from the full-field hygro-expansion, where the θ is (expected to approximate) the MFA

In order to validate if the MFA is lower for RD compared to FD HW fibers and if the MFA is reversible after the "transformation", an (second) independent MFA measurement method is required such as used by Liu et al. (2016). Unfortunately, as discussed above, this method is difficult to employ. To validate the second mechanism, i.e. the lower longitudinal hygro-expansivity of the micro-fibrils due to the storage of dried-in strain in the dislocated cellulose regions. Freely and RD nano-fibrillated cellulose, which does not contain an MFA, thereby separating the two mechanisms, should be prepared. Subsequent single fibril hygro-expansion characterization, using Atomic Force Microscopy, similar to Lee et al. (2010), may elucidate (longitudinal) hygro-expansivity differences between FD and RD fibrils.

The SW fiber are studied next to investigate whether the above discussed theories and findings for HW fibers are also applicable to the SW fibers.

Softwood fibers

The regular strains together with the principal strain computation of the SW fibers are given in Fig. 7. Let us first consider RH cycles 1−2. The SW fibers show both positive and negative values for θ, which are outside of the MFA range reported in the literature, i.e. 8−39 (Barnett and Bonham 2004; Cown et al. 2004). This suggests that other mechanisms affect the direction of the deformation, which will be studied in the following.

Regarding the reversibility of the release of dried-in strain, remarkably, the shrinkage and principal strain components of the RD SW fibers in Fig. 7 remain (nearly) unchanged after the wetting cycle (t-test: all quantities are statistically not different within 98% confidence). Thus, the RD SW fibers do not "transform" to fibers exhibiting the characteristics of FD SW fibers, in contrast to the

HW fibers. The only difference in testing procedure between the HW and SW fibers was the duration of the wetting cycle, which was, most of the times, longer for the HW fibers, see Fig. 1a. Therefore, the time dependence of the release of dried-in strain is investigated next.

Moisture-induced "transformation" from restrained to freely dried fibers

A droplet of water (200 μL) was applied to three randomly selected RD SW fibers from the fibers shown in Fig. 7, and placed in a 100% RH environment for 12 h, to maintain the fiber fully soaked. Note that the fibers were still fixed on the glass substrate by the nylon wires. The fibers were afterwards again patterned (as most of the pattern is washed away when the water was removed) and subsequently subjected to two RH cycles of 30−90−30% (cycles 5−6). The average strain change during drying from 90 to 30%, i.e. $\bar{\epsilon}_{ll}^-$, $\bar{\epsilon}_{tt}^-$, and $\bar{\epsilon}_{lt}^-$ (with standard deviation) of RH cycles 3−4 (after the wetting cycle during the initial experiments) and RH cycles 5−6 of the three fibers is given in Fig. 8 (Case I). The average FD SW fiber shrinkage and standard deviation of RH cycles 1−2 shown in Fig. 7a ($\bar{\epsilon}_{ll}^{FD-}$, $\bar{\epsilon}_{tt}^{FD-}$, and $\bar{\epsilon}_{lt}^{FD-}$) are added for reference. The fibers do not show a significant change in shrinkage. In short, soaking RD SW fibers for 12 h does not induce a "transformation" to FD SW fibers.

To compliment the analysis, the twist of 25 randomly extracted fibers from each FD and RD, HW and SW handsheets was characterized. The SW fibers showed an average fiber twist of 0.60 ± 0.37 and 0.08 ± 0.04 rot/mm for FD and RD respectively, while the HW fibers showed a much lower difference in twist between FD and RD, i.e., 0.08 ± 0.05 and 0.05 ± 0.04 rot/mm respectively. After immersing each fiber in a droplet of water for 12 h (while being completely unconstrained on a teflon sheet), the twist of the SW fibers increased to 0.80 ± 0.39 and 0.38 ± 0.18 rot/mm for FD and RD, respectively, and the HW fibers remained about constant at 0.09 ± 0.0 0.06 ± 0.04 rot/mm for FD and RD, respectively. The key finding is that the fiber twist of the RD SW fibers significantly increases after being soaked for a longer time, whereas the RD HW fibers do not. Hence, it is likely that the RD SW fibers require twisting in order to "transform" into a FD SW fiber and the RD HW fibers do not, which is consistent with the SW fibers'
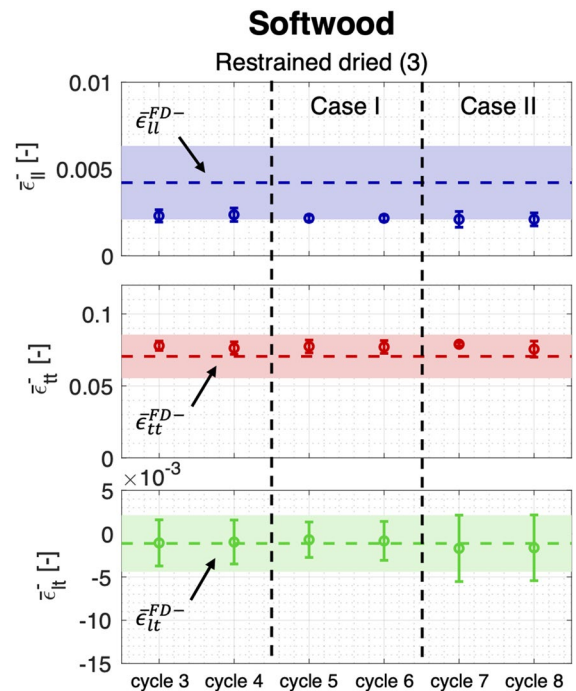

Fig. 8 The change in $\bar{\epsilon}_{ll}^-$, $\bar{\epsilon}_{tt}^-$, and $\bar{\epsilon}_{lt}^-$ with standard deviation of three randomly selected RD SW fibers before and after soaking the fiber in water for 12 h, while (i) being constrained by the nylon wires in water for 12 h (Case I), and (ii) being completely free for 12 h (Case II), also allowing the fiber to twist. $\bar{\epsilon}_{ll}^-$, $\bar{\epsilon}_{tt}^-$, and $\bar{\epsilon}_{lt}^-$ of the FD SW fibers considering RH cycles 1−2 including their standard deviation, as given in Table A.1, are denoted by the horizontal dashed lines and bands

larger MFA compared to HW (French et al. 2000; Barnett and Bonham 2004; Cown et al. 2004; Donaldson 2008). Additionally, the increase in twist may indicate increased longitudinal stress, as this is converted into twisting due the MFA of the fiber. Hence, the minor constraint by the nylon threads may still have prevented the RD SW fibers from "transforming" into FD SW fibers after being soaked for 12 h, as the fibers are only allowed to minimally rotate during the hygro-expansion experiments, and not the necessary twist increase of ∼ 0.3 rot/mm as measured in the fiber twist study.

Therefore, the three SW RD fibers (from Case I) were again soaked in water for 12 h, but this time without nylon threads making them completely free to twist. Note that all dry fibers demonstrated an increased fiber twist after being soaked without constraints, comparable to the numbers from the fiber twist study. These fibers were patterned, re-clamped

by the threads, and subjected to two RH cycles from 30−90−30% (cycles 7−8). $\bar{\epsilon}_{ll}^-$, $\bar{\epsilon}_{tt}^-$, and $\bar{\epsilon}_{lt}^-$ (with standard deviation) of the three fibers are given in Fig. 8 (Case II). Note that none of the fibers show a significant change in shrinkage, and did not "transform" to FD SW fibers. Only a small increase in $\bar{\epsilon}_{lt}$ was found, which may logically be caused by the increased twist that the fibers now exhibit. It is possible that a mechanical activation (e.g. stirring) is required to structurally 'transform' the RD SW fibers into FD SW fibers. Therefore, the fiber structure is studied next.

To further explore the "transformation" from RD to FD fibers, the elastic stiffness of the fibers can also be studied. It is known that FD fibers yield a lower stiffness than RD fibers (Jentzen 1964). Hence to validate if fibers are hygroscopic and mechanically reversible, the elastic properties of RD fibers before and after wetting should be studied.

The fiber's structural differences

In Fig. 5, it is observed that the SW fibers exhibit a significantly lower $\bar{\epsilon}_{lt}^-$ than the HW fibers (for both RD and FD), even after soaking, considering that the helically-shaped micro-fibrils require to slide along each other to allow the hemi-cellulose to swell, and that the SW fiber's MFA is much larger than the HW fibers' (French et al. 2000; Barnett and Bonham 2004; Cown et al. 2004; Donaldson 2008). Additionally, $\bar{\epsilon}_{ll}^-$ of the SW fibers is only slightly higher than the HW fibers, where a much larger difference is expected according to the findings of Meylan (1972) and Yamamoto et al. (2001) for wood fibers. Therefore, it seems that the SW fibers tested here are somehow constrained in their movement. A plausible explanation could be that the lumen of the SW fibers are all (partially) collapsed.

For a collapsed lumen, the top and bottom cell wall are bonded to each other, in which the direction of the micro-fibrils of the bottom cell wall are crossed (under an angle of 2 times the MFA) with the top cell wall, restricting the fiber to shear and expand. This is in contrast to an open lumen case, which is more typical for wood fibers, thus explaining the difference between the present results and those of Meylan (1972) and Yamamoto et al. (2001). A collapsed lumen may also explain the larger averaged value and variation in ϵ_{ll}^- and ϵ_{lt}^- for FD compared to RD SW

fibers (see Fig. 7a). In the RD SW case, the lumen could logically more often be closed (compared to FD), restricting the ϵ_{ll}^- and ϵ_{lt}^- of the fiber, resulting in similar values. Whereas for the FD SW fibers the lumen may sometimes be open, resulting in a larger scatter in ϵ_{ll}^- and ϵ_{lt}^-. Such a hypothesis agrees well with the findings by He et al. (2003), who showed that larger drying pressures result in more frequent closed lumens, or sections of the lumen being closed. Considering the HW fibers, the frequency of a closed lumen is expected to be much less compared to the SW fibers, based on the higher fiber wall stiffness of the HW fibers having both a thicker cell wall and smaller fiber radius (Ilvessalo-Pfäffli 1995; Antes and Joutsimo 2015), making the structure less prone to collapsing. In contrast to the SW fibers which have a thin cell wall and large fiber radius (Lundqvist et al. 2002), which is consistent with the width to thickness ratio of, respectively, 3.2 ± 1.5 and 5.9 ± 3.1 for the HW and SW fibers tested here. Finally, a collapsed lumen of the SW fibers could also explain why the apparent MFA in Fig. 7b is approximately 0 degrees, because the top and bottom wall, which deform almost equally, constrain each other. As the lumen of the HW fibers may not be collapsed, the top and bottom fiber walls are free to swell perpendicular to the micro-fibrils, resulting in a major-minor strain direction, i.e. MFA, corresponding to literature values.

In summary, all these reasons make it quite plausible that the larger $\bar{\epsilon}_{lt}^-$ and minor difference in $\bar{\epsilon}_{ll}^-$ of the HW compared to SW fibers is because the lumen of the SW fibers is more often closed than the HW fibers due to the difference in the fiber's stiffness. To extend this theory towards the storage of dried-in strains, it is possible that closing the lumen during restrained drying locks the dried-in strain into the fibers, and the lumen needs to be (mechanically) opened in order to release the dried-in strain. This hypothesis may explain why the RD HW fibers are able to "transform" into FD HW fibers, whereas the RD SW fibers cannot. The details of the lumen of the fibers is therefore studied next.

Lumen analysis: experimental

In order to study if the lumen of a fiber is (partially) open or closed, the change of the shape of the fiber is studied. For instance, the cross-sectional shape of an open lumen fiber is more likely to change when

Fig. 9 Change in cross-sectional shape of five FD and RD, HW and SW fibers characterized at three positions along the fiber length, before (blue) and after soaking (red) the fiber in water for 12 h
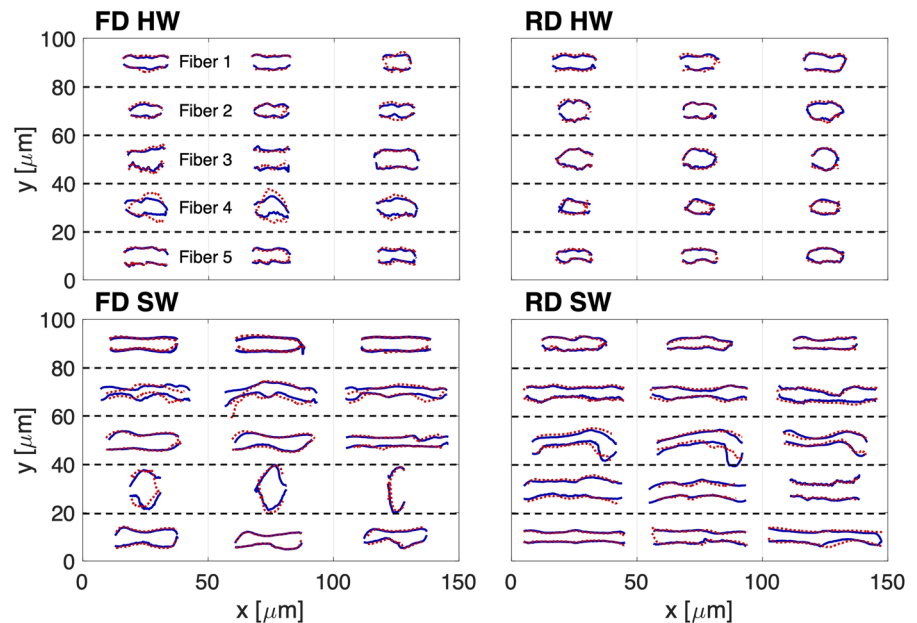
the fiber is analyzed before and after being soaked in water, while for a closed lumen, the shape is less likely to change. Hence, Fig. 9 displays the shape of five FD and RD, HW and SW fibers (randomly extracted from the handsheets) at three different locations along the fiber length (at 25, 50 and 75% of the fiber length) is analyzed before (blue) and after (red) being soaked in water for 12 h. Details on the experimental methodology can be found in Subsection "Lumen analysis: fiber cross-sectional shape" (Supplementary information).

Three fiber sections are displayed per row for every fiber. The significant differences in fiber cross-sectional dimensions between the HW and SW fibers are directly visible. None of the HW fibers have a flat shape, both for FD and RD, suggesting their open structure. The FD and RD SW fibers on the other hand have a much flatter structure, except for FD SW fiber 4, which most likely has an open structure. The RD SW fibers seem to be closed before and after soaking, visualized by their flat shape which remains unchanged. This may explain why the hygro-expansivity of the RD SW fibers does not change after soaking, because the soaking treatment did not open the lumen.

The FD SW fibers also seem mostly closed except for fiber 4, suggesting that, on average, the FD SW fibers are less closed than the RD SW fibers. Moreover, most of the FD SW fibers show, to some extent,

a shape change (more than RD SW fibers), which suggests that the top and bottom can (partially) slide along each other. Perhaps the micro-fibrils decorating the top and bottom inside wall are entangled, keeping the lumen from completely opening, while still allowing some relative motion. The partial sliding ability of the top and bottom wall of the FD SW fibers would explain why the apparent MFA of the FD SW fibers, displayed in Fig. 7b, is higher than that of RD SW fibers, but still significantly lower than the MFA values reported in literature.

This method enabled characterization of cross-sectional shape of the fiber before and after wetting. To analyze the shape of the lumen, a microtome can be used, similar to Kappel et al. (2009). This however does require embedding the fiber into a resin, and water soaking will not be possible.

Lumen analysis: numerical

This above-described theory is validated using a numerical fiber model, of which a schematic representation along with the details are described in Subsection "Numerical fiber model" (Supplementary information). Two extreme cases are considered, i.e. a fully open fiber and fully closed fiber. The effect of the fiber width to thickness (*w/t*) is studied for a range from 3 to 10, similar to the cross-sections in
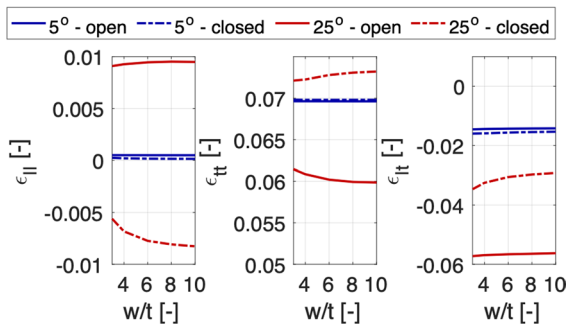
Fig. 10 The longitudinal (ϵ_{ll}), transverse (ϵ_{tt}), and shear (ϵ_{lt}) hygro-expansion of an open and closed fiber structure. An MFA of 5 and 25° representing the average MFA of, respectively, HW and SW, and a width to thickness ratio (w/t) of 3−10 is studied. A schematic representation and details of the fiber model can be found in Subsection "Numerical fiber model" (Supplementary information)

Fig. 9. Additionally, an MFA of 5° or 25°, which are the average MFA values for, respectively, the HW and SW fibers tested here (French et al. 2000; Barnett and Bonham 2004; Cown et al. 2004; Donaldson 2008), are modeled. The ϵ_{ll}, ϵ_{tt}, and ϵ_{lt} at the fiber's top surface is plotted versus the w/t ratio, for a closed and open lumen, and MFA, in Fig. 10.

First of all, the solutions tend to converge for increasing w/t ratios. As expected, for an open lumen, ϵ_{ll}, and ϵ_{lt} increase for a larger MFA, similar to the wood fibers characterized by Meylan (1972) and Yamamoto et al. (2001), whereas ϵ_{tt} logically decreases. Interestingly, closing the lumen results in a decrease in ϵ_{ll}, and ϵ_{lt}, which is most significant for the large MFA cases, where ϵ_{ll} even becomes negative. Hence, this model suggests that ϵ_{ll} and ϵ_{lt} decrease with increasing degree of bonding. Taking into account that the closed lumen model is of course an overestimation of the degree of internal fiber bonding (assumed to be driven by the same mechanisms as inter-fiber bonding, i.e. never perfectly bonded (Hirn and Schennach 2015)), may explain why the SW fibers, in spite of their significantly larger MFA, exhibit a similar ϵ_{ll} as the HW fibers. The model also suggests that the large scatter in ϵ_{ll}^{-} and ϵ_{lt}^{-} of the FD compared to the RD SW fibers displayed in Fig. 7 is driven by the lumen of the FD SW fibers being (partially) closed/open, while the lumen of the RD fibers is more often closed. Finally, the result that a closed lumen can induce a negative ϵ_{ll} is confirmed by the SW pulp fiber tested in (Vonk et al. 2021), which
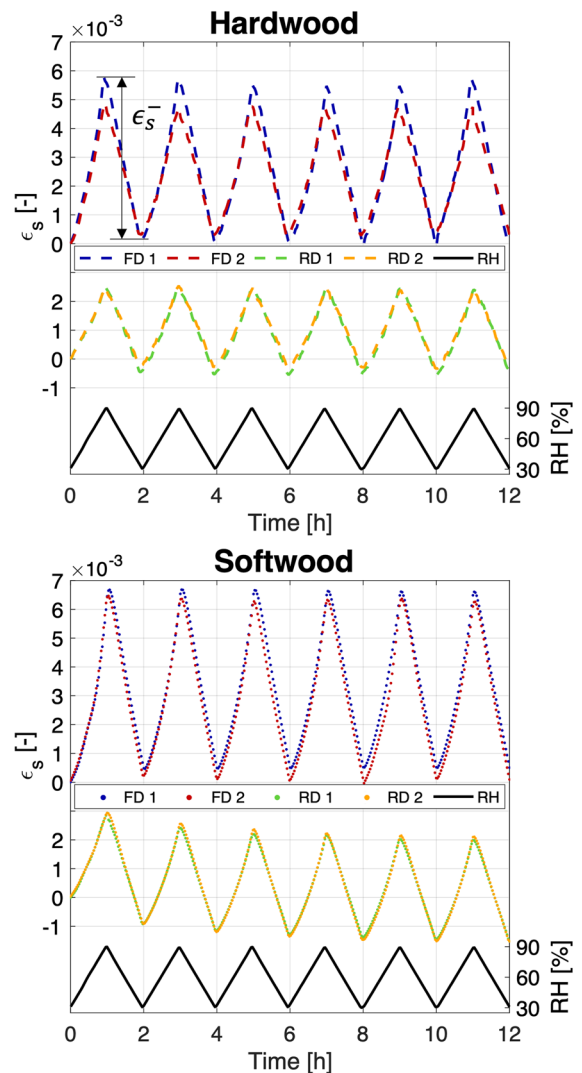

Fig. 11 The isotropic hygro-expansion response (ϵ_s) of two FD and RD SW and HW handsheets. The hygro-expansivity of (i) FD handsheets is significantly larger than then RD, and (ii) the SW handsheets is larger than the HW, both similar to literature (Uesaka et al. 1992; Uesaka and Moss 1997; Larsson and Wågberg 2008; Urstöger et al. 2020). The shrinkage during each drying slope from 90 to 30% RH, as annotated (ϵ_s^{-}) in RH cycle 1 of HW FD1, is extracted and given in Table A.2

exhibited a negative ϵ_{ll}. Note that the proposed model does not predict the same hygro-expansion values as found in this work, as it lacks on some key aspects, i.e., non-continuous helical structure, no expansion along the micro-fibrils, no multiple cell wall layers., etc. so care should be taken into the interpretation of these results.

In summary, the above-conducted experimental and numerical analyses suggests that HW fibers, on average, have open lumen structures, and therefore exhibit (i) a relatively large longitudinal and shear hygro-expansion with a low MFA, similar to open wood fibers, and (ii) the "transformation" from a RD to a FD fiber can occur. The SW fibers, in which the lumen is partially closed for FD, and more often closed for RD, exhibit (i) a relatively low longitudinal and shear hygro-expansivity with a high MFA, in contrast to their wood fiber counterparts, and (ii) no "transformation" occurs from RD to FD.

Even though the above-described experimental-numerical fiber structure analysis reveals some factors affecting the fiber hygro-expansivity, other mechanisms may have to be explored in order to fully understand the observation made in this work. Hygro-expansion experiments need to be conducted on fibers of which the full structure, i.e. fiber dimensions, MFA, and lumen geometry, is known upfront. This also enables more elaborate modeling, similar to Joffre et al. (2016), in contrast to the simplified model used here. Additionally, the chemical composition, i.e. hemi-celluloses and lignin contents may also be required upfront as they also affect the fiber hygro-expansivity (Lindner 2018). Finally, the thickness of the S1 and S3 layer may also play a significant role in the storage of dried-in strain in the fibers, consequently affecting the fiber hygro-expansion.

Fiber-to-sheet coupling

From modeling it is known that the longitudinal fiber hygro-expansion is dominant and fully contributes to the sheet hygro-expansion, while the transverse fiber strain contributes through the bonds (Brandberg et al. 2020). In order to experimentally validate this and separate the longitudinal and transverse fiber strain contributions to the sheet scale, the sheet-scale hygro-expansion evolution of the FD and RD, HW and SW handsheets, from which the fibers were extracted, is characterized and presented in Fig. 11.

The strains in both directions were equal for every RH cycle of every handsheet test, indicating the expected isotropic hygro-expansivity of the handsheets and the reliability of the measurement method. The isotropic sheet-scale hygro-expansion (ϵ_s) response of the two RD and FD SW and HW handsheets is given in Fig. 11. The curves are in

line with other sheet-scale hygro-expansion works, e.g., the RD handsheets show a clear release of irreversible dried-in strain after the wetting slope of the first RH cycles, whereas the FD handsheets do not (Uesaka et al. 1992; Niskanen et al. 1997; Larsson and Wågberg 2008). Additionally, the RD SW handsheets display an ongoing release of dried-in strain characterized by every peak or valley per cycle is lower than the previous, in contrast to RD HW.

The average handsheet shrinkage (ϵ_s^-) per handsheet, considering all six drying slopes as annotated for the first cycle (ϵ_s^-), and the total average handsheet shrinkage ($\bar{\epsilon}_s^-$) considering both handsheets per pulp and drying procedure are given in Table A.2. $\bar{\epsilon}_s^-$ is also added to the longitudinal fiber strain plot in Fig. 5. $\bar{\epsilon}_s^-$ reveals that the HW and SW handsheets exhibit a factor 1.72 ± 0.24 and 1.72 ± 0.06 larger hygro-expansivity between FD and RD respectively (t-test: both are statistically different within 98% confidence), consistent with literature (Uesaka et al. 1992; Uesaka and Moss 1997; Larsson and Wågberg 2008; Urstöger et al. 2020). Furthermore, the SW handsheets exhibit a larger shrinkage than HW for RD and FD (t-test: both are statistically different within 98% confidence), similar to the longitudinal and transverse fiber shrinkage presented in Fig. 5. After adding $\bar{\epsilon}_s^-$ to the corresponding $\bar{\epsilon}_{ll}^-$ plot in Fig. 5, it is found that $\bar{\epsilon}_{ll}^-$ is close to the sheet-scale expansivity for every handsheet type, indicating that the contribution of the longitudinal fiber hygro-expansion to the handsheet is dominant, while the transverse strain contribution is relatively weak, which complies with model results (Uesaka 1994; Motamedian and Kulachenko 2019; Brandberg et al. 2020).

From the fiber network model proposed by Brandberg et al. (2020), a simple rule of mixture calculation can be used to upscale the fiber characteristics, given in Table A.1, to find the sheet-scale hygro-expansivity, i.e., $1 \cdot \epsilon_{ll} + 0.0375 \cdot \epsilon_{tt} = \epsilon_s$ (($\beta_s(= 0.0525) - \beta_{ll}(= 0.03))/\beta_{ll}(= 0.60) = 0.0375$ in (Brandberg et al. 2020)). For HW the predicted sheet-scale hygro-expansion is 0.0064 ± 0.0005 and 0.0038 ± 0.0009 for FD and RD, respectively, while for SW, it is 0.0068 ± 0.0027 and $0.0051 + 0.0026$ for FD and RD respectively. These predictions are slightly larger than the actual sheet-scale hygro-expansions given in Table A.2. Moreover, the model predicts that the HW and SW handsheets exhibit a factor 1.67 ± 0.52 and 1.33 ± 1.20 larger hygro-expansivity between the FD

and RD, respectively, whereas the experiment shows somewhat larger values, i.e. 1.72 ± 0.24 and 1.72 ± 0.06 respectively. The small differences may be attributed to the difference in paper structure between the model and experiment, i.e., fiber coverage, grammage, fiber geometry, etc., all affecting the model's outcome.

The fact that (i) the longitudinal fiber hygro-expansion is indeed dominant at the sheet scale, (ii) the longitudinal fiber hygro-expansion is strongly reduced by the RD process, and (iii) the dried-in strain stored inside the SW fibers is difficult to release is actually beneficial for digital printing purposes. Indeed any decrease of the hygro-expansivity of the fibers directly reduces the severity of the unwanted out-of-plane deformations such as cockling, fluting, waviness, and curl.

Conclusion

The significantly larger hygro-expansivity of freely compared to restrained dried paper sheets has been frequently studied in the literature. Various theories or hypotheses have been forwarded to explain these differences, including the geometry of the inter-fiber bonds and the structural fiber changes due to the drying procedure. The latter theory is studied in this work by testing the hygro-expansion of fibers extracted from freely and restrained dried handsheets.

To this end, restrained dried and freely dried handsheets were produced from either hardwood or softwood fibers. The hygro-expansion of the handsheets was obtained using a novel sheet-scale hygro-expansion method. Single fibers were extracted from the remainder of the handsheets which were tested using a recently-developed single fiber hygro-expansivity method which captures the transient full-field (longitudinal, transverse and shear) hygro-expansion during relative humidity (RH) changes. Each fiber was subjected to (i) two 30−90−30% RH cycles, then (ii) a wetting cycle in which the RH is increased to 95% for a longer time, while the fiber is cooled down, initiating hydro-expansion and maximizing the fiber's moisture content, and finally (iii) two 30−90−30% RH cycles. This strategy is chosen to see if a restrained dried fiber is able to "transform" into a freely dried fiber.

The freely dried handsheets exhibit a significantly larger hygro-expansivity than the restrained dried. Furthermore, it was found that the restrained drying procedure mainly lowers the fibers' longitudinal hygro-expansion, which is dominant at the sheet-scale hygro-expansion, hence explaining the sheet-scale hygro-expansion differences. Regarding the hardwood fibers:

- Computation of the principal strains revealed that the major-minor strain angle (perpendicular to the micro-fibrils) and the minor strain (along the micro-fibrils) is lower for restrained dried, hence the lower longitudinal hygro-expansion,
- The lower minor strain of restrained dried fibers compared to the freely dried fibers confirm an older theory from the literature,
- All fibers were able to "transform" from restrained to freely dried.

Regarding the softwood fibers:

- The principal strain computation did not show any change in the major-minor strain angle between the freely and restrained dried fibers,
- The fibers were not able to "transform" from a restrained to a freely dried fiber, even after immersing the fiber in water in an unconstrained condition for long periods.

To study the driving mechanisms of the differences between hardwood and softwood fibers, the fibers' cross-sectional shape before and after wetting was investigated experimentally and numerically to elucidate the influence of the lumen. On average, the lumen of the hardwood fibers seemed to be open, while the softwood fibers are more often closed. For softwood, the micro-fibrils of the top and bottom wall are crossed and bonded, which (i) restrict free hygro-expansion, resulting in different major-minor strain angles, and (ii) restricts the release of dried-in strain, which requires the lumen to be open in order to be released. Finally, the strength of testing single fibers from handsheets enables a direct comparison between the fiber and sheet properties, and it was found that the transverse fiber hygro-expansion contribution to the sheet scale is relatively low.

Data availability The presented data will be made available on request.

Declarations

Conflict of interest The authors declare that they have no known competing financial interests or personal relationships that could have appeared to influence the work reported in this work.

Consent of publication The authors hereby consent to publication of the present research work in this journal, if selected for publication.

Ethics approval This article does not contain any studies with human participants or animals performed by any of the authors.

References

Agarwal UP, Ralph SA, Reiner RS, Baez C (2016) Probing crystallinity of never-dried wood cellulose with raman spectroscopy. Cellulose 23:125–144. https://doi.org/10.1007/s10570-015-0788-7

Agarwal UP, Reiner RR, Ralph SA (2013) Estimation of cellulose crystallinity of lignocelluloses using near-ir ft-raman spectroscopy and comparison of the raman and segal-waxs methods. J Agric Food Chem 61:103–113. https://doi.org/10.1021/jf304465k

Alzweighi M, Mansour R, Tryding J, Kulachenko A (2022) Evaluation of hoffman and xia plasticity models against bi-axial tension experiments of planar fiber network materials. Int J Solids Struct 238:111358. https://doi.org/10.1016/j.ijsolstr.2021.111358

Anagnost SE, Mark RE, Hanna RB (2002) Variation of microfibril angle within individual tracheids. Wood Fiber Sci 1:337–349

Antes R, Joutsimo OP (2015) Fiber surface and paper technical properties of eucalyptus globulus and eucalyptus nitens pulps after modified cooking and bleaching. BioResources 10:1599–1616. https://doi.org/10.15376/biores.10.1.1599-1616

Barnett JR, Bonham VA (2004) Cellulose microfibril angle in the cell wall of wood fibres. Biol Rev 79:461–472. https://doi.org/10.1017/S1464793103006377

Berglund LA (2011) 12. wood biocomposites–extending the property range of paper products, In: Mechanics of paper products. De Gruyter, pp 231–254. https://doi.org/10.1515/9783110254631.231

Brandberg A, Motamedian HR, Kulachenko A, Hirn U (2020) The role of the fiber and the bond in the hygro-expansion and curl of thin freely dried paper sheets. Int J Solids Struct 193:302–313. https://doi.org/10.1016/j.ijsolstr.2020.02.033

Brecht W, Gerspach A, Hildenbrand W (1956) Drying tensions, their influence on some paper properties. Das Pap 10:454–458

Brecht W, Gerspach A, Hildenbrand W (1956) Tensions on drying and their effects on various paper properties. Das Pap 10:454–458

Cave ID (1997) Theory of x-ray measurement of microfibril angle in wood. Wood Sci Technol 31:225–234. https://doi.org/10.1007/BF00702610

Courchene CE, Peter GF, Litvay J (2006) Cellulose microfibril angle as a determinant of paper strength and hygro-expansivity in pinus taeda l. Wood Fiber Sci 1:112–120

Cown DJ, Ball RD, Riddell MJC (2004) Wood density and microfibril angle in 10 pinus radiata clones: distribution and influence on product performance. N Z J For Sci 34:293

Czibula C, Brandberg A, Cordill MJ, Matković A, Glushko O, Czibula C, Kulachenko A, Teichert C, Hirn U (2021) The transverse and longitudinal elastic constants of pulp fibers in paper sheets. Sci Rep 11:1–13. https://doi.org/10.1038/s41598-021-01515-9

De Böck R, van de Ven AAF, Saes LH, Maubach JML, Koren B (2017) Moisture-induced buckling of paper sheets, analysis and simulation. Int J Solids Struct

128:296–308. https://doi.org/10.1016/j.ijsolstr.2017.08.038

Donaldson L (2008) Microfibril angle: measurement, variation and relationships-a review. Iawa J 29:345–386. https://doi.org/10.1163/22941932-90000192

Fahlén J, Salmén L (2005) Pore and matrix distribution in the fiber wall revealed by atomic force microscopy and image analysis. Biomacromolecules 6:433–438. https://doi.org/10.1021/bm040068x

Fellers C (2007) The interaction of paper with water vapour, vol 2. Walter de Gruyter, Berlin

French J, Conn AB, Batchelor WJ, Parker IH (2000) The effect of fibre fibril angle on some handsheet mechanical properties. Appita J 53:210–215

Gorisek Z, Torelli N (1999) Microfibril angle in juvenile, adult and compression wood of spruce and silver fir. Phyton 39:129–132

Haslach HW (2000) The moisture and rate-dependent mechanical properties of paper: a review. Mech Time-Depend Mater 4:169–210. https://doi.org/10.1023/A:1009833415827

He J, Batchelor WJ, Johnston RE (2003) The behavior of fibers in wet pressing. Tappi J 2:27–31

Heinemann S, Retulainen E (2014) Microfibril angles of softwood and hardwood pulp fibres measured with white-light polarimetry. In: Progress in paper physics seminar, PPPS 2014

Hirn U, Bauer W (2006) Investigating paper curl by sheet splitting. In: Proceedings of the 2006 Eucepa supported conference 'Challenges in Pulp-and Papermaking Technology'. Bratislava, Slovakia

Hirn U, Schennach R (2015) Comprehensive analysis of individual pulp fiber bonds quantifies the mechanisms of fiber bonding in paper. Sci Rep 5:1–9. https://doi.org/10.1038/srep10503

Hubbe MA (2014) Prospects for maintaining strength of paper and paperboard products while using less forest resources: A review. BioResources 9:1634–1763. https://doi.org/10.15376/biores.9.1.1634-1763

Hubbe MA, Venditti RA, Rojas OJ (2007) What happens to cellulosic fibers during papermaking and recycling? A review. BioResources 2:739–788. https://doi.org/10.15376/biores.2.4.739-788

Ilvessalo-Pfäffli MS (1995) Fiber atlas: identification of papermaking fibers. Springer Science & Business Media, Cham

Jentzen CA (1964) The effect of stress applied during drying on some of the properties of individual pulp fibers. Dissertation, Georgia Institute of Technology

Joffre T, Isaksson P, Dumont PJJ, Rolland du Roscoat S, Sticko S, Orgéas L, Gamstedt EK (2016) A method to measure moisture induced swelling properties of a single wood cell. Exp Mech 56:723–733. https://doi.org/10.1007/s11340-015-0119-9

Jordan L, Daniels RF, Clark A III, He R (2005) Multilevel nonlinear mixed-effects models for the modeling of earlywood and latewood microfibril angle. For Sci 51:357–371

Kappel L, Hirn U, Bauer W, Schennach R (2009) A novel method for the determination of bonded area of individual fiber-fiber bonds. Nord Pulp Pap Res J 24:199–205. https://doi.org/10.3183/npprj-2009-24-02-p199-205

Kouko J, Retulainen E, Kekko P (2014) Influence of straining during wet pressing and drying on strength properties of paper. Nordic Pulp Pap Res J 29:453–461. https://doi.org/10.3183/npprj-2014-29-03-p453-461

Kulachenko A, Denoyelle T, Galland S, Lindström SB (2012) Elastic properties of cellulose nanopaper. Cellulose 19:793–807. https://doi.org/10.1007/s10570-012-9685-5

Kulachenko A, Gradin P, Uesaka T (2005) Tension wrinkling and fluting in heatset web offset printing process. post buckling analyses. In: 13th fundamental research symposium on advances in paper science and technology Location: Univ Cambridge, Cambridge, ENGLAND Date: SEP, 2005, The Pulp and Paper Fundamental Research Society. pp 1075–1099

Larsson PA, Hoc M, Wågberg L (2009) The influence of grammage, moisture content, fibre furnish and chemical modifications on the hygro-and hydro-expansion of paper. In: 14th fundamental research symposium on advances in pulp and paper research location: St Annes Coll, Oxford, ENGLAND Date: SEP 13-18, 2009, pp 355–388

Larsson PA, Wågberg L (2008) Influence of fibre-fibre joint properties on the dimensional stability of paper. Cellulose 15:515–525. https://doi.org/10.1007/s10570-008-9203-y

Lee JM, Pawlak JJ, Heitmann JA (2010) Longitudinal and concurrent dimensional changes of cellulose aggregate fibrils during sorption stages. Mater Charact 61:507–517. https://doi.org/10.1016/j.matchar.2010.02.007

Liitiä T, Maunu SL, Hortling B (2000) Solid state nmr studies on cellulose crystallinity in fines and bulk fibres separated from refined kraft pulp. Holzforschung 54:618–624. https://doi.org/10.1515/HF.2000.104

Lindner M (2018) Factors affecting the hygroexpansion of paper. J Mater Sci 53:1–26. https://doi.org/10.1007/s10853-017-1358-1

Liu J, Kim JI, Cusumano JC, Chapple C, Venugopalan N, Fischetti RF, Makowski L (2016) The impact of alterations in lignin deposition on cellulose organization of the plant cell wall. Biotechnol Biofuels 9:1–17. https://doi.org/10.1186/s13068-016-0540-z

Lundqvist SO, Ekenstedt F, Grahn T, Wilhelmsson L (2002) A system of models for fiber properties in Norway spruce and scots pine and tools for simulation. Proc IUFRO S 5:01–04

Magnusson MS, Östlund S (2013) Numerical evaluation of interfibre joint strength measurements in terms of three-dimensional resultant forces and moments. Cellulose 20:1691–1710. https://doi.org/10.1007/s10570-013-9939-x

Mäkelä P (2009) Effect of drying conditions on the tensile properties of paper. In: Transactions of the 14th fundamental research symposium Oxford, pp 1079–1094

Meylan BA (1972) The influence of microfibril angle on the longitudinal shrinkage-moisture content relationship. Wood Sci Technol 6:293–301. https://doi.org/10.1007/BF00357051

Motamedian HR, Kulachenko A (2019) Simulating the hygroexpansion of paper using a 3d beam network model and concurrent multiscale approach. Int J Solids Struct 161:23–41. https://doi.org/10.1016/j.ijsolstr.2018.11.006

Nanko H, Wu J (1995) Mechanisms of paper shrinkage during drying. International paper physics conference. Niagara-on-the-Lake, Canada, pp 103–113

Nanri Y, Uesaka T (1993) Dimensional stability of mechanical pulps: drying shrinkage and hygroexpansivity. Tappi J 76:62–66

Neagu RC, Gamstedt EK, Bardage SL, Lindström M (2006) Ultrastructural features affecting mechanical properties of wood fibres. Wood Mater Sci Eng 1:146–170. https://doi.org/10.1080/17480270701195374

Neggers J, Blaysat B, Hoefnagels JPM, Geers MGD (2016) On image gradients in digital image correlation. Int J Numer Methods Eng 105:243–260. https://doi.org/10.1002/nme.4971

Niskanen KJ, Kuskowski SJ, Bronkhotst CA (1997) Dynamic hygroexpansion of paperboards. Nordic Pulp Pap Res J 12:103–110. https://doi.org/10.3183/npprj-1997-12-02-p103-110

Page DH, Tydeman PA (1962) A new theory of the shrinkage, structure and properties of paper. Form Struct Pap 1:397–425

Retulainen E, Niskanen KJ, Nilsen N (1998) Fibers and bonds, vol 2. Fapet Oy, Helsinki

Salmén L (1982) Temperature and water induced softening behaviour of wood fiber based materials. Dissertation, Royal Institute of Technology Stockholm

Salmén L, Boman R, Fellers C, Htun M (1987) The implications of fiber and sheet structure for the hygroexpansivity of paper. Nordic Pulp Pap Res J 2:127–131. https://doi.org/10.3183/npprj-1987-02-04-p127-131

Salmén L, Fellers C, Htun M (1987) The development and release of dried-in stresses in paper. Nordic Pulp Pap Res J 2:44–48. https://doi.org/10.3183/npprj-1987-02-02-p044-048

Sarén MP, Serimaa R (2006) Determination of microfibril angle distribution by x-ray diffraction. Wood Sci Technol 40:445–460. https://doi.org/10.1007/s00226-005-0052-7

Shafqat S, Hoefnagels JPM (2021) Cool, dry, nano-scale dic patterning of delicate, heterogeneous, non-planar specimens by micro-mist nebulization. Exp Mech 61:917–937. https://doi.org/10.1007/s11340-020-00686-2

Smith SF (1950) Dried-in strains in paper sheets and their relation to curling, cockling and other phenomena. Pap Maker Br Pap Trade J 1:185–192

Uesaka T (1994) General formula for hygroexpansion of paper. J Mater Sci 29:2373–2377. https://doi.org/10.1007/BF00363429

Uesaka T, Moss C (1997) Effects of fiber morphology on hygroexpansivity of paper-a micromechanics approach. Fundam Papermak Mater 1:663–679

Uesaka T, Moss C, Nanri Y (1992) The characterization of hygroexpansivity of paper. J Pulp Pap Sci 18:J11–J16

Uesaka T, Qi D (1994) Hygroexpansivity of paper: effects of fibre-to-fibre bonding. J Pulp Pap Sci 20:J175–J179

Urstöger G, Kulachenko A, Schennach R, Hirn U (2020) Microstructure and mechanical properties of free and restrained dried paper: a comprehensive investigation. Cellulose 27:8567–8583. https://doi.org/10.1007/s10570-020-03367-4

Van den Akker JA (1961) Some theoretical considerations on the mechanical properties of fibrous structures. In: Symposium transactions, technical section of the British paper and board Maker's association

Vonk NH, Geers MGD, Hoefnagels JPM (2021) Full-field hygro-expansion characterization of single softwood and hardwood pulp fibers. Nordic Pulp Pap Res J 36:61–74. https://doi.org/10.1515/npprj-2020-0071

Vonk NH, Peerlings RHJ, Geers MGD, Hoefnagels JPM (2023a) Full-field, quasi-3d hygroscopic characterization of paper inter-fiber bonds. arXiv preprint arXiv:2304.10507

Vonk NH, Peerlings RHJ, Geers MGD, Hoefnagels JPM (2023b) Re-understanding the in-plane hygro-expansion of freely and restrained dried paper handsheets. In: 17th fundamental research symposium (in preparation)

Vonk NH, van Spreuwel WPC, Anijs T, Peerlings RHJ, Geers MGD, Hoefnagels JPM (2023c) Transient hygro-and hydro-expansion of freely and restrained dried paper: the fiber-network coupling. arXiv preprint arXiv:2303.15480

Vonk NH, Verschuur NAM, Peerlings RHJ, Geers MGD, Hoefnagels JPM (2020) Robust and precise identification of the hygro-expansion of single fibers: a full-field fiber topography correlation approach. Cellulose 27:6777–6792. https://doi.org/10.1007/s10570-020-03180-z

Wahlström T (2009) Development of paper properties during drying, vol 2. Walter de Gruyter, Berlin

Wang HH, Drummond JG, Reath SM, Hunt K, Watson PA (2001) An improved fibril angle measurement method for wood fibres. Wood Sci Technol 34:493–503. https://doi.org/10.1007/s002260000068

Yamamoto H, Sassus F, Ninomiya M, Gril J (2001) A model of anisotropic swelling and shrinking process of wood. Wood Sci Technol 35:167–181. https://doi.org/10.1007/s002260000074

Ye C, Sundström MO, Remes K (1994) Microscopic transmission ellipsometry: measurement of the fibril angle and the relative phase retardation of single, intact wood pulp fibers. Appl Opt 33:6626–6637. https://doi.org/10.1364/AO.33.006626

Zhang W, Fei B, Tian G, Hu T, Yue X, Chang Y, Jiang Z et al (2019) Comparative study on physical mechanic properties of phyllostachys edulis in different latitudes. J Beijing For Univ 41:136–145. https://doi.org/10.13332/j.1000-1522.20180245